J Mater Sci (2009) 44:1054–1062
DOI 10.1007/s10853-008-3186-9

Compressibility and compactibility studies of chitosan, xanthan gum, and their mixtures

Ala'a F. Eftaiha · Musa I. El-Barghouthi · Iyad S. Rashid · Mayyas M. Al-Remawi · Abdullah I. Saleh · Adnan A. Badwan

Received: 22 September 2008 / Accepted: 11 December 2008 / Published online: 14 January 2009

Abstract The compressibility and compactibility studies of binary mixtures containing chitosan (CS) and xanthan gum (XG) were highlighted in this article. The compressibility of the examined powders was studied according to Heckel and Gurnham equations. Results indicated that CS exhibits more ductile character than XG. Moreover, in this study percolation theory has been applied to the tensile strength of different compacts obtained from CS–XG mixtures. The obtained percolation thresholds showed that higher pressures must be applied to form compacts with a specific strength as the mass fraction of XG was increased. Additionally, the values of the maximum tensile strength showed that the percolation threshold of CS occurs at equal mass fraction of the two polymers. Scanning electron microscope, light microscope techniques, and molecular mechanical calculations were also conducted in order to study the interactions between CS and XG. The obtained results revealed that 1:1 ratio (by weight) represents the maximum interactions between the two polymers.

Introduction

Solid binary mixtures are gaining ground interests to be used in the controlled release of drugs. Different factors are considered to achieve optimum formulas such as polymer-to-polymer ratio and drug-to-polymeric mixture ratios [1]. However, the determination of these parameters is time consuming due to a large number of experimental studies required. Therefore, alternative approaches have to be considered in order to minimize the amount of experimental study. One of these approaches is the percolation theory [2], which has mainly been used to explain compacts formation, the behavior of controlled release dosage forms and fast disintegrating tablets. It was found that system properties divert, vanish, or start to appear at certain composition [3–29].

Tablet formation can be considered as a combination of site and bond percolation phenomena [3, 17, 30]. Generally, when particles or granules are poured into machinery dies prior to compaction, the lattice sites are either empty forming pores or occupied by particles forming clusters. During the uniaxial compression, the number of lattice sites to be finally occupied is continuously reduced until the final dimension of the tablet is achieved. Thus, at the beginning of the compaction process, bond percolation is responsible for stress transmission and it could be identified at a lower percolation threshold corresponding to the relative tapped density [20]. Following particles rearrangement, a significant buildup of stress occurs as particles can no longer be displaced easily. This situation is typical for a site percolation process [9].

Leuenberger et al. [3, 8, 20] used the percolation theory for the determination of the percolation threshold of binary mixtures with different mechanical properties. One specific focus of their study investigated the relationship between the tap density and the composition of powder binary mixtures composed of Lactose-Avicel® and Emcompress-Avicel®, observing two inflecting points corresponding to the percolation threshold of components [8]. Furthermore,

A. F. Eftaiha · M. I. El-Barghouthi (✉) · A. I. Saleh
Department of Chemistry, The Hashemite University, P.O. Box 150459, Zarqa 13115, Jordan
e-mail: musab@hu.edu.jo

I. S. Rashid · M. M. Al-Remawi · A. A. Badwan
Suwagh Drug Delivery Systems, Subsidiary of the Jordanian Pharmaceutical Manufacturing Co., Naor, Jordan

A. A. Badwan
e-mail: jpm@go.com.jo

they examined the maximum tensile strength and the compressibility parameter as a function of mass fraction of a binary mixture of polyethylene glycol and lactose. They observed that the component that percolates the system controls its mechanical properties [3].

A binary mixture consisting of a well-compactible and a poorly compactable substance, microcrystalline cellulose and paracetamol, respectively, was also studied, and a method for the determination of the dilution capacity, which is useful for the formulation of direct compressible mixtures [6], was established.

Additionally, the activity loss of compacted β-galactosidase with microcrystalline cellulose was interpreted using the percolation theory. According to this study, the amount of β-galactosidase tablets with a plastic excipient should not fall below 20% to minimize activity loss [27].

Hydrophilic polymers such as chitosan (CS) and xanthan gum (XG) are used in formulating tablets for immediate or controlled release [31–38]. The main hindrance for their use is their flowability and compressibility [39], which may hamper their use. Consequently, a systematic study to explore the appropriate concentration of each component is becoming important.

The main objective of this study is to determine the proper concentration to formulate controlled release preparation by studying some mechanical properties of these hydrophilic polymers using percolation theory. Different mixtures of CS and XG were prepared to examine their compressibility, compaction properties, and how the fractions of each component affect the mechanical properties of the compacts. The extent of interaction between these compounds was examined theoretically and experimentally by molecular modeling and scanning electron microscopy, respectively.

Experimental

Materials and chemicals

Chitosan: viscosity (0.5% (w/v) in 0.1 M HCl) 16.80 mPa s, percentage of deacetylation 93%, average particle size 174.0 μm, pharmaceutical grade (Batch No. HJ 040411) from Hong Ju, China.

Xanthan gum: viscosity (0.5% (w/v) in water) 40.7 mPa s, average particle size 106.7 μm, food and pharmaceutical grade (Batch No. 2504519) from Jungbanzlauer Ges. M.B.H. Handelsgericht Wien, Germany. All other reagents used were of analytical grade.

Instruments

Universal testing machine: RKM50, PRÜF system, Germany; *Hydraulic Press*: with press cage, Shimadzu, Japan; *Digital caliper*: Vernier caliper; *Hardness tester*: Copley, Nottm Ltd, Switzerland; *Helium pycnometer*: Ultrapycnometer 1000, Quatachrome Co., USA; *High-speed gas sorption analyzer*: Quantachrome Co., NOVA 2200, USA; *Tap Volumeter*: SVM, Erwika, Germany; *Scanning electron microscope* (*SEM*): FEI Quanta 200, Netherlands; *Particle size analyzer*: Masetrsizer 2000, Malvern Instruments Ltd., UK.

Compacts preparation and testing

Different mixtures of CS and XG containing 0, 20, 50, 67, 80, and 100% (mass percent) of CS were prepared. The powder mixtures were mixed geometrically for 5 min. Compacts were prepared by uniaxial direct compression using a universal testing machine. The upper and lower punches and the die were not lubricated, and the compression rate was 30 mm/min. The applied compaction pressure ranged from 25 to 390 MPa. Three tablets were compressed from each composition at each compaction pressure to ensure reproducibility. Flat, round tablets with 12-mm-diameter, and weight of 400 mg were produced. Compacts thickness was measured out of die after compaction using a digital caliper after a storage time of 48 h in sealed vials. Hardness of compacts was measured using hardness tester; tablets that showed ideal fracture were taken into account. The radial tensile strength was calculated according to the following equation [6]:

$$\sigma_t = 2F/(\Pi Dh), \quad (1)$$

where σ_t is the radial tensile strength, F the maximal force recorded, D the tablet diameter, and h is the tablet thickness.

Surface area measurement

The surface areas of CS and XG were determined using the high-speed gas sorption analyzer, whereby 2 g of each sample was used. The equipment bath temperature was set at −195.4 °C using liquid nitrogen. The adsorption and desorption setup was fixed at a tolerance of 0.1 mmHg and equilibrium time of 60 s.

Density determination

Bulk density

Bulk density of the examined powders was calculated from geometrical dimensions, where a specific amount of powder was poured in a cylinder and the volume of powder was taken as the bulk volume.

Tapped density

The tapped density of examined powders was determined with a mechanical tapping device. Two to four grams of powder (according to the bulk density) was subjected to 100 taps. If the volume of powder was changed significantly, another 100 taps were applied. The volume of the powder was read off as being the tap volume. The tapped density was calculated by dividing the powder mass on the powder volume.

True density

True density of each component was measured using Helium pycnometer. The true density of the mixtures was determined according to the following equation [40]:

$$(1/D_t) = (\chi_1/D_1) + (\chi_1/D_2), \quad (2)$$

where χ_i and D_i are the mole fraction and the true density of each component, respectively.

Relative bulk density and relative tapped density were calculated as the ratio of bulk and tapped density to true density, respectively.

Porosity was calculated according to the following relation, $\varepsilon = 1 - \rho$, where ε is porosity and ρ is the relative density.

Films preparation of CS, XG, and their mixtures

For films preparation, different concentrations of XG (0.25 and 0.5% (w/v) in 0.05 M NaOH) and CS (0.5 and 1% (w/v) in 0.1 M HCl) were prepared under stirring. The solutions were degassed by sonication. These solutions were used for preparing films as follows.

The XG solution was added at the minimum amount needed to cover the Petri dish in the form of a thin layer on which CS solution was poured. Mixtures in the Petri dishes were left for 2 h in order to ensure complete reaction between CS and XG. Any adsorbed species were washed away using sufficient amount of distilled water to remove non-reacted species.

The prepared films were CS, XG, 2:1, 1:1, and 1:2 of CS-to-XG ratio by weight.

Scanning electron microscopy

Samples were fixed on aluminum stubs and then coated with gold by sputtering at 1200 V, 20 mA for 105 s using vacuum coater. The samples were studied using solid-state detector for back-scattered electrons.

Molecular modeling

Calculations in vacuum were performed with Hyperchem® (release 6.03 professional, Hyperchem Inc., Waterloo, Canada) using Amber force field. The structures of D-glucosamine(s) hydrochloride (the building unit of Chitosan Hydrochloride) and one monomer unit of XG were built up from standard bond lengths and angles and then minimized. The numbers of D-glucosamine hydrochloride units studied were in the range from 1 to 10 monomer unit, where each combination with the monomer unit of XG represents a specific weight ratio. In order to reach the lowest energy of the D-glucosamine(s) hydrochloride-XG complex, each time the minimized structures of D-glucosamine hydrochloride unit(s) and one monomer unit of XG were merged, then geometry optimization was conducted for the whole system. After interaction, the minimum potential energy of D-glucosamine hydrochloride unit(s) alone was identified after running geometry optimization.

The binding energy (E_{binding}) was calculated according to the following equation [41]:

$$E_{\text{binding}} = E_{(\text{D-glucosamine hydrochloride-xanthan gum})} - \left(E_{(\text{Free D-glucosamine hydrochloride})} + E_{(\text{Free xanthan gum})}\right) \quad (3)$$

Results and discussion

Compressibility of CS, XG, and their mixtures

Table 1 lists density characterization of CS, XG, and their mixtures. The values of relative bulk and tapped density showed that CS is more porous than XG, where ε_B and ε_T (porosity of the bulk and the tapped powder, respectively) for CS is 0.879 and 0.842 while for XG is 0.571 and 0.510.

Load–displacement curves for different mixtures of CS and XG are shown in Fig. 1. CS showed higher volume reduction than XG especially in the first region. This is due to less interparticle voids between XG particles compared to CS as indicated above. This means that particle rearrangement has played more important role in compact formation of CS compared to XG, which turned CS into a more suitable ingredient to facilitate compression. Moreover, Fig. 1 shows that the step of particle rearrangement seemed to have more contribution in compact formation when the mass fraction of CS was increased. Furthermore, the compression cycle of 1:1 (w/w) CS-XG was closer to the cycle of XG cycle than CS.

Figure 2 shows Heckel plots for CS, XG, and their mixtures of die. The low-pressure region of Heckel plot (i.e., <35 MPa) showed that CS formed the most porous compacts, as indicated earlier. However, >35 MPa, CS formed the least porous compacts and XG formed the most porous compacts.

Table 1 Density characterization of CS, XG, and their mixtures

Mass fraction of CS	True density (g/cm^3)	Bulk density (g/cm^3)	Relative bulk density	Tapped density (g/cm^3)	Relative tapped density
1.00	1.5849[a]	0.192	0.121	0.250	0.158
0.80	1.5953[b]	0.221	0.138	0.284	0.178
0.67	1.6021[b]	0.242	0.151	0.315	0.196
0.50	1.6111[b]	0.286	0.177	0.376	0.233
0.20	1.6273[b]	0.513	0.315	0.584	0.359
0.00	1.6382[a]	0.700	0.429	0.801	0.490

[a] Measured experimentally

[b] Estimated form Eq. 2

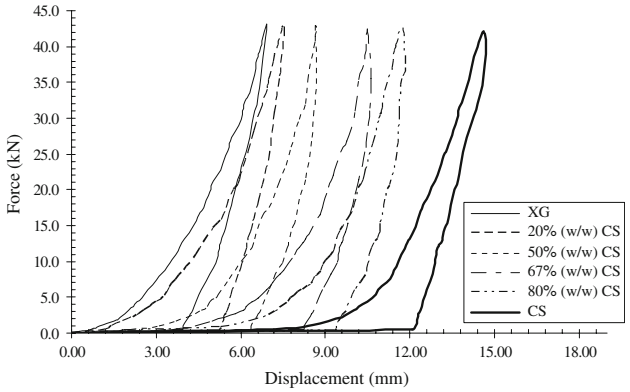

Fig. 1 Load–displacement curves for different mixtures of CS and XG

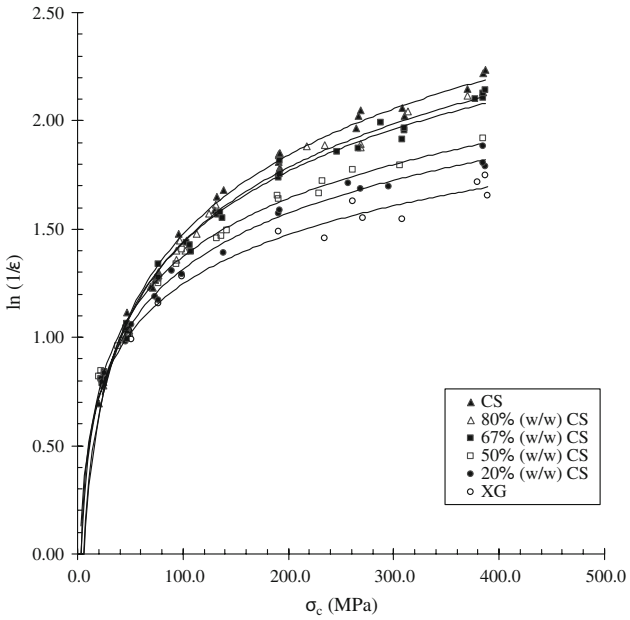

Fig. 2 Heckel plots for CS, XG, and their mixtures of die

The Gurnham equation [42] was used to study the contribution of plastic deformation in compacts formation for different mixtures of CS and XG. According to Gurnham's model,

Table 2 c values and correlation coefficient obtained from Gurnham equation of CS, XG, and their mixtures

Mass fraction of CS	c	r^2
1.00	13 ± 1.4	0.992
0.80	13.1 ± 0.71	0.993
0.67	11.7 ± 0.55	0.992
0.50	11.2 ± 0.56	0.993
0.20	10.7 ± 0.55	0.993
0.00	8.7 ± 0.78	0.991

$$\varepsilon(\%) = -c \ln \sigma_c + d, \tag{4}$$

where c and d are constants. The constant c (slope), which obtained by plotting ε (%) versus ln σ_c, provides a good representation of material compressibility. Higher c values indicate better compressibility [43]. Table 2 lists the obtained c values for different mixtures of CS and XG. Zhao et al. [43] classified lactose monohydrate, dibasic calcium phosphate dihydrate, and acetaminophen as brittle materials (c is 9.06, 8.16, and 6.41, respectively), whereas corn starch and microcrystalline cellulose were classified as ductile materials (c is 17.62 and 16.78, respectively). Therefore, according to Zhao's classification XG ($c = 8.7 \pm 0.78$) is a brittle material, whereas CS ($c = 13 \pm 1.4$) is a ductile material. Furthermore, plasticity was found to increase as the mass fraction of CS was increased (Table 2).

Compactibility of CS and XG

Percolation theory treats the compacts formation by using scaling law [6]:

$$\sigma_t = k(\rho - \rho_c)^{T_f}, \tag{5}$$

where k is the scaling factor, T_f is the fracture exponent. Guyon et al. [44] proposed a theoretical value for the fracture exponent, i.e., $T_f = 2.7$. The same value of critical exponent was used in the current study.

Setting the tensile strength to the inverse power of the exponent T_f (Eq. 5), a straight line would be obtained with slope a and intercept b [6]:

$$\sigma_t^{1/T_f} = k^{1/T_f}(\rho - \rho_c) = a\rho + b. \quad (6)$$

Thus, the percolation threshold ρ_c is equal to $-b/a$. Table 3 lists the values of strength percolation threshold (ρ_c) and correlation coefficient (r^2) of CS, XG, and their mixtures obtained from the corresponding plots of $\sigma_t^{0.37}$ versus ρ. Results in Table 3 indicate that adjacent particles of CS bonded to each other to form a compact having relevant bonding strength at a lower relative density than XG particles (ρ_c (CS) < ρ_c (XG)). This can be verified using the data of specific surface area of CS and XG, which were 2.13 and 0.22 m^2/g, respectively. Thus, the contact surface area between CS molecules would be larger than that of between XG molecules during compression, and hence higher intermolecular bonding between CS molecules compared to XG molecules at any compaction pressure. Results in Table 3 also show that the strength percolation threshold was found to increase with decreasing mass fraction of CS. This is expected due to the fact that CS is the strength producing part in the mixtures.

Figure 3 represents tensile strength versus relative densities for CS and XG and their mixtures. Sudden changes in the behavior of tensile strength could be interpreted as the relative densities at which pores start to form isolated clusters (pores percolation threshold), where particles inside compacts were not easily displaced. Pores percolation threshold is the relative density at the intersection point between the two lines representing the two regions of each plot as shown in Fig. 3. A plot of pores percolation threshold against mass fraction of CS is shown in Fig. 4. The plot is composed of three regions, where the behavior of solid fraction against pores is changed dramatically between 66.7 and 50% (w/w) of CS. Thus, below 50% (w/w) of CS, the behavior of solid fraction resembled XG, i.e., XG particles encapsulated CS particles. Above 66.7% (w/w) of CS, the behavior of solid fraction resembled CS, i.e., CS formed infinite cluster(s) and XG formed isolated clusters. While between 66.7 and 50% (w/w) of CS, both of them spanned through the whole system.

Maximum tensile strength (σ_{tmax}) of CS, XG, and their mixtures was deduced from exponential extrapolation of the tensile strength when $\rho \to 1$, the obtained values were plotted versus mass fraction of CS (Fig. 5). Figure 5 illustrates that there is a sudden change in the σ_{tmax} of mixtures when the mass fraction of CS around 50% (w/w).

Table 3 Strength percolation threshold (ρ_c) and linear regression data of CS, XG, and their mixtures according to Eq. 6

Mass fraction of CS	a	b	ρ_c	r^2
1.00	3.6293	−1.2229	0.337	0.991
0.80	3.8057	−1.4373	0.378	0.992
0.67	3.5713	−1.3637	0.382	0.991
0.50	3.5661	−1.4384	0.403	0.990
0.20	3.9515	−1.8343	0.464	0.991
0.00	3.9789	−1.9448	0.489	0.989

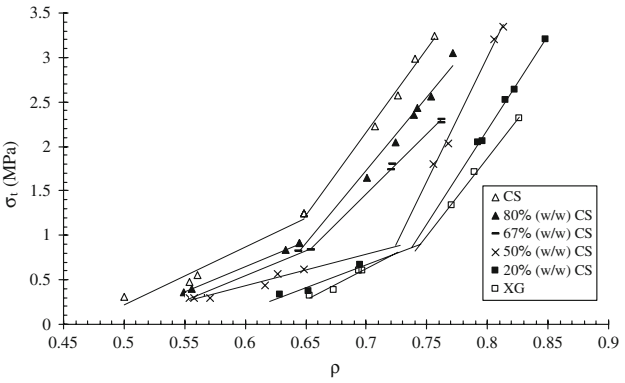

Fig. 3 Tensile strength (σ_t) as a function of relative density for CS, XG, and their mixtures

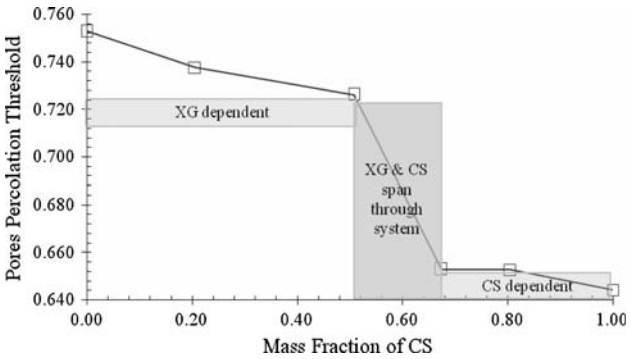

Fig. 4 The estimated values of pores percolation threshold against mass fraction of CS

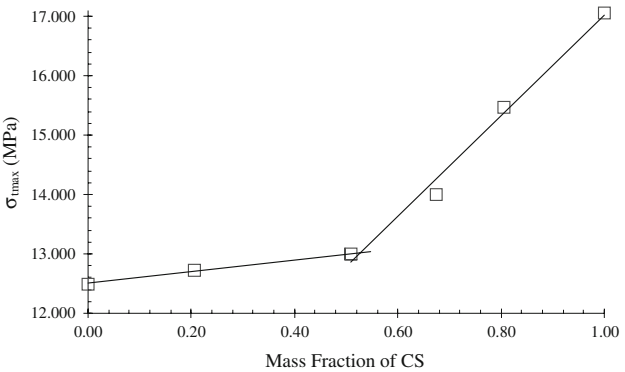

Fig. 5 Plot of maximum tensile strength versus the mass fraction of CS

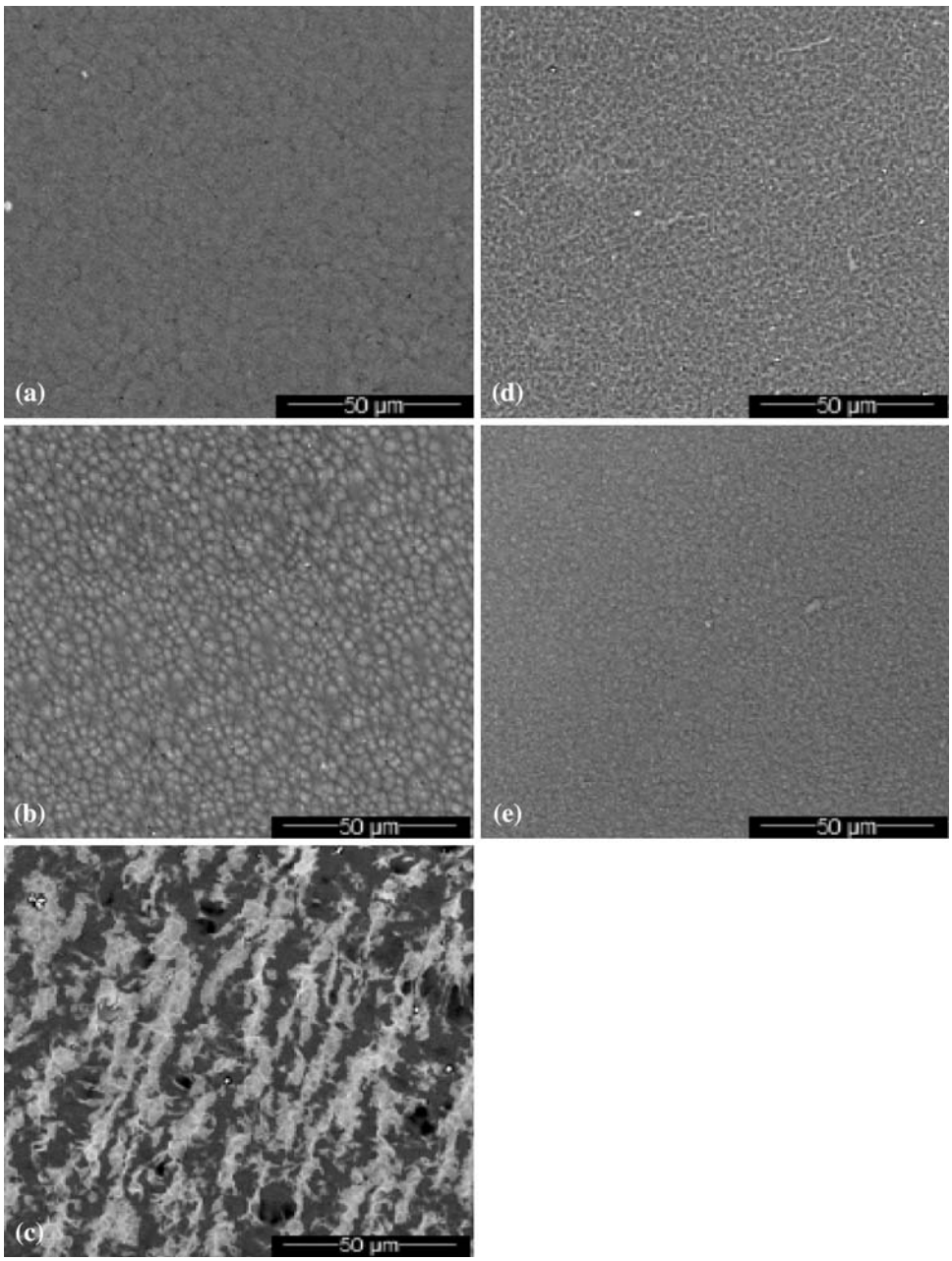

Fig. 6 SEMs corresponding to films for different mixtures of CS and XG using solid-state detector for back-scattered electrons. Magnification 2000×. **a** CS at pH = 1, **b** CS-XG (2:1), **c** CS-XG (1:1), **d** CS-XG (1:2), and **e** XG at pH = 1

Thus, at low mass fraction of CS, where finite clusters were dispersed in an infinite XG cluster, σ_{tmax} values increased slowly, implying that σ_{tmax} values were not affected by the concentration of CS. When the mass fraction of CS exceeded 50%, σ_{tmax} increased steeply with increasing the mass fraction of CS. This point is the percolation threshold of CS, which indicates the existence of infinite cluster of CS and XG. Theoretically, a second inflection point corresponding to the percolation threshold of XG should be deduced from the plot. However, no other sharp deviation was recognizable indicating that crossover of XG clusters from infinite to finite or vice versa, hardly affected any change and thus did not cause the relationship to diverge. Basically, in the presence of infinite cluster of CS, the infinite cluster of XG played a subordinate role in determining the tensile strength of the compact, attributable to the fact the CS is more compactable than XG.

SEM and molecular modeling

CS-XG (1:1) (w/w) was developed as a controlled release matrix for solid dosage forms [38]. This combination develops an insoluble hydrogel layer during dissolution process that occurs at the surface of a tablet, which leads to the formation of an insoluble coat that retards the release of drugs [38]. The extent of interaction between CS and XG in

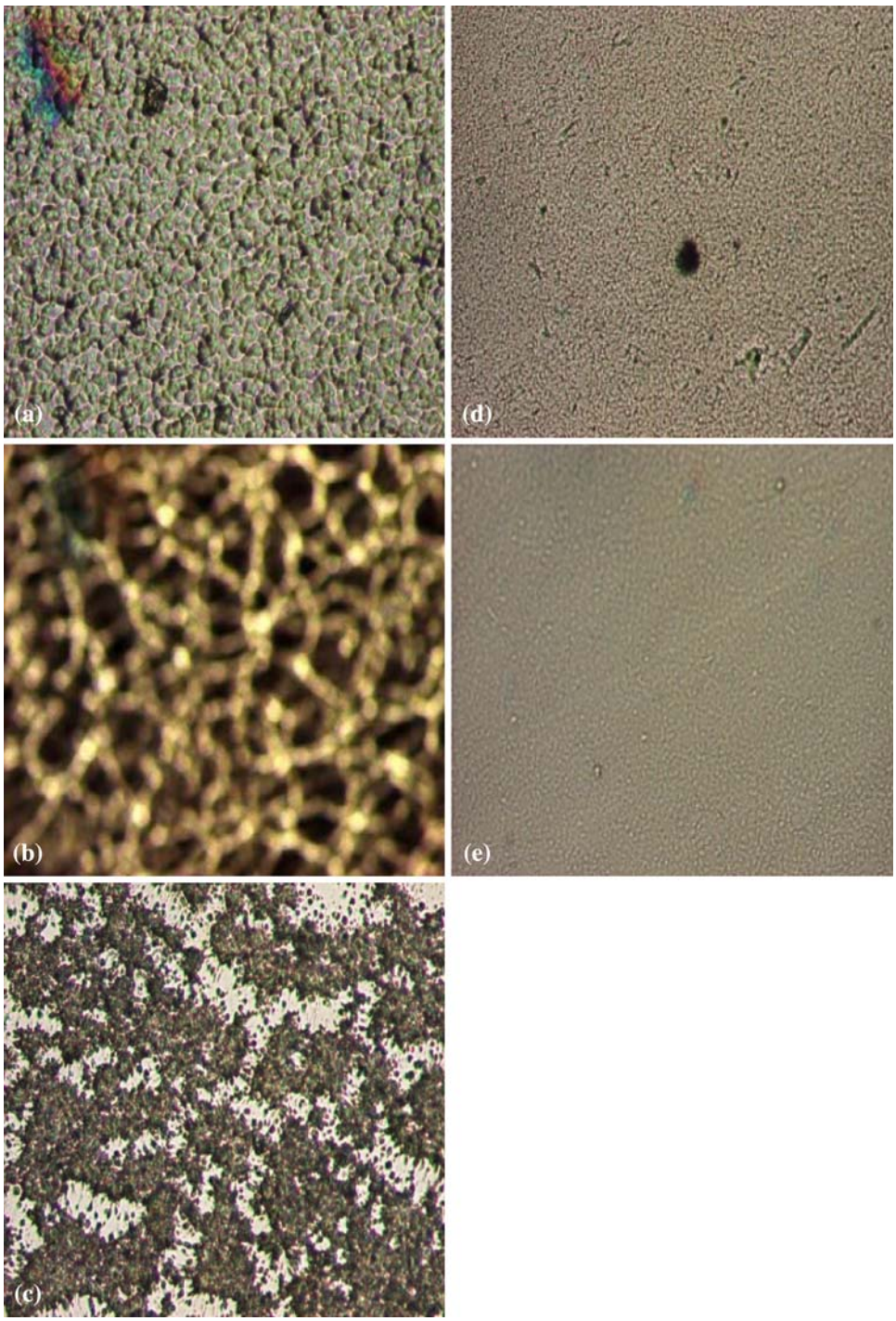

Fig. 7 Micrographs corresponding to films of: **a** CS at pH = 1, **b** CS-XG (2:1), **c** CS-XG (1:1), **d** CS-XG (1:2), and **e** XG at pH = 12 using light microscope. Magnification 400×

liquid state was studied by examining the morphology of the formed hydrogel by SEM and light microscope (Figs. 6 and 7).

CS appears with a rough surface (Fig. 6a); the roughness appears clearly using light microscope (Fig. 7a), whereas the surface of XG (Figs. 6e and 7e) appears smooth. When the interaction between CS and XG took place, and upon the formation of the hydrogel, the morphology of the surface changed dramatically depending on the degree of interactions. Figures 6 and 7 (b and d) show a rough surface that represents the formed hydrogel in a fibrous form that was dispersed between CS and XG particles, respectively. Figures 6c and 7c show the hydrogel, which appears in light gray, and pores that appear in dark gray. This hydrogel appears to be losing its integrity. These figures reveal a maximum interaction between CS and XG at this weight ratio (1:1) compared with 2:1 and 1:2 (w/w) CS-XG. Therefore, SEM suggests that the 1:1 weight ratio

Table 4 The computed binding energy of different weight ratios of GlcN · HCl to XG

No. of D-glucosamine unit	Mass ratio of (GlcN · HCl:XG)	Binding energy (kcal/mol)
1	1:5.28	−262.31
2	1:2.64	−308.25
3	1:1.73	−353.78
4	1:1.32	−358.34
5	1:1.06	−438.49
6	1:0.88	−397.21
7	1:0.75	−421.0
8	1:0.66	−386.55
9	1:0.59	−426.16
10	1:0.53	−395.16

showed the maximum interaction and hence maximum retardation of drugs upon using it as a controlled released matrix.

In order to better understand the interaction between CS and XG, molecular mechanics calculations using AMBER force field were conducted. Although the molecular weights of the interacting molecules are far below those used in compaction studies, this preliminary method predicts the interaction by assuming what occurs on monomer level can be extended to the polymer level. The binding energies of a different number of D-glucosamine hydrochloride (GlcN · HCl) units with one monomer unit of XG are presented in Table 4. The results indicate that the 1:1 mixture (w/w) exhibits the maximum interaction between GlcN · HCl and XG in agreement with previous experimental work by Badwan et al. [38], and with the results of SEM.

Conclusions

Percolation theory has been used with great interest in the design of dosage forms. In this study, percolation theory has been applied to the tensile strength of CS-XG compacts. The obtained critical relative densities are understood as strength percolation thresholds. Results showed that the strength percolation threshold was found to increase with decreasing the mass fraction of CS. The percolation threshold between the two is achieved at 1:1 (w/w). Below this point CS is encapsulated inside XG particles and above it, CS and XG span through the whole system. The interaction between CS and XG was examined experimentally using SEM and light microscope and theoretically by molecular mechanics. These studies indicated that when CS-to-XG ratio was 1:1 (w/w); a maximum interaction between them was achieved. Figure 8 shows the

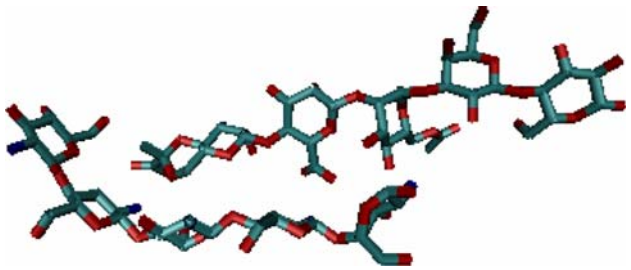

Fig. 8 View of the molecular complex formed between five monomer units of D-glucosamine with one monomer unit of XG

view of the molecular complex formed between five monomer units of Gln with one monomer unit of XG.

Acknowledgement The Authors would like to thank Prof. Hans Leuenberger from University of Basel-Switzerland and Dr. Abeer Shnoudh from Philadelphia Private University-Jordan for reading the manuscript and for their helpful discussions.

References

1. Mehta KA, Kislalioglu MS, Phuapradit W, Malick AW, Shah NH (2002) Pharm Technol 26:26
2. Stauffer D, Aharony A (1994) Introduction to percolation theory. Taylor and Francis Ltd, London
3. Leuenberger H, Rohera BD, Hass Ch (1987) Int J Pharm 38:109
4. Leuenberger H, Bonny JD, Kolb M (1995) Int J Pharm 115:217
5. Leuenberger H (1999) Adv Powder Technol 10:323
6. Kuentz M, Leuenberger H (2000) Eur J Pharm Biopharm 49:151
7. Holman LE, Leuenberger H (1988) Int J Pharm 46:35
8. Holman LE, Leuenberger H (1990) Powder Technol 60:249
9. Holman LE, Leuenberger H (1991) Powder Technol 64:233
10. Leuenberger HA, Bonny JD (1991) Pharm Acta Helv 66:160
11. Bonny JD, Leuenberger H (1993) Pharm Acta Helv 68:25
12. Caraballo I, Fernández-Arévalo M, Holgado MA, Rabasco AMM (1993) Int J Pharm 96:175
13. Caraballo I, Fernández-Arévalo M, Holgado MA, Rabasco AM, Leuenberger H (1994) Int J Pharm 109:229
14. Caraballo I, Millán M, Rabasco AM, Leuenberger H (1996) Int J Pharm 71:335
15. Caraballo I, Fernández-Arévalo M, Millán M, Rabasco AM, Leuenberger H (1996) Int J Pharm 139:177
16. Caraballo I, Melgoza LM, Alvarez-Fuentes J, Soriano MC, Rabasco AM (1999) Int J Pharm 181:23
17. Lue R, Leuenberger H (1993) Int J Pharm 90:213
18. Luginbühl R, Leuenberger H (1994) Pharm Acta Helv 69:127
19. Fernández-Hervás MJ, Vela MT, Holgado MA, Cerro J, Rabasco AM (1995) Int J Pharm 113:39
20. Leuenberger H, Ineichen L (1997) Eur J Pharm Biopharm 44:269
21. Melgoza LM, Caraballo I, Alvarez-Fuentes J, Millán M, Rabasco AM (1998) Int J Pharm 170:169
22. Melgoza LM, Rabasco AM, Sandoval H, Caraballo I (2001) Eur J Pharm Biopharm 12:453
23. Tongwen X, Binglin H (1998) Int J Pharm 170:139
24. Soriano MC, Caraballo I, Millán M, Piñero RT, Melgoza LM, Rabasco AM (1998) Int J Pharm 174:63
25. Kuentz M, Leuenberger H, Kolb M (1999) Int J Pharm 182:243
26. Kuentz M, Leuenberger H (2000) Powder Technol 111:145
27. Kuny T, Leuenberger H (2003) Int J Pharm 260:137
28. Busignies V, Leclerc B, Porion P, Evesque P, Couarraze G, Tchorelo P (2006) Eur J Pharm Biopharm 64:51

29. Busignies V, Leclerc B, Porion P, Evesque P, Couarraze G, Tchorelo P (2007) Eur J Pharm Biopharm 67:507
30. Blattner D, Kolb M, Leuenberger H (1990) Pharm Res 7:113
31. Gupta KC, Ravi Kumar MNV (2000) J Appl Polym Sci 76:672
32. Mitrevej A, Sinchaipanid N, Rungvejhavuttivittaya Y, Kositchaiyong V (2001) Pharm Dev Technol 6:385
33. El-Gazayerly ON (2003) Drug Dev Ind Pharm 29:241
34. Mu X, Tobyn MJ, Staniforth JN (2003) Drug Dev Ind Pharm 29:19
35. Rowe RC, Sheskey PJ, Weller PJ (2003) Handbook of pharmaceutical excipients. The Pharmaceutical Press, London
36. Agnihotri SA, Aminabhavi TM (2004) J Control Release 96:245
37. Berger J, Reist M, Mayer JM, Felt O, Peppas NA, Gurny R (2004) Eur J Pharm Biopharm 57:19
38. Badwan AA, Al-Remawi MA, Salem MB (2005) EP Patent 1512394, 9 Mar 2005
39. Freyer KMP, Brink D (2006) AAPS PharmSciTech 7(3):75
40. Imbert C, Tchoreloff P, Leclerc B, Couarraze G (1997) Eur J Pharm Biopharm 44:273
41. El-Barghouthi MI, Masoud NA, Al-Kafawein JK, Zughul MB, Badwan AA (2005) J Incl Phenom Macro Chem 53:15
42. Gurnham CF, Masson HJ (1946) Ind Eng Chem 38:1309
43. Zhao J, Burt HM, Miller RA (2006) Int J Pharm 17:109
44. Guyon E, Roux S, Bergman D (1987) J Phys 48:903